View metadata, citation and similar papers at core.ac.uk

brought to you by CORE

provided by The University of Utah: J. Willard Marriott Digital Library

DOES LONG-TERM PROTEIN PHOSPHATASE 2A INHIBITION IN MICE DYSREGULATE PERIPHERAL GLUCOSE HOMEOSTASIS, LOWER HEPATIC GLYCOGEN CONTENT, AND IMPAIR INSULIN-MEDIATED SIGNAL TRANSDUCTION IN THE LIVER?

by

Juyeon Lee

A thesis submitted to the faculty of
The University of Utah
in partial fulfillment of the requirements for the degree of

Master of Science

Department of Exercise and Sport Science

The University of Utah

December 2016

Copyright © Juyeon Lee 2016

All Rights Reserved

The University of Utah Graduate School

STATEMENT OF THESIS APPROVAL

The thesis of **Juyeon Lee**

has been approved by the following supervisory committee members:

John David Symons	, Chair	**9.20.2016** Date Approved
Thunder Jalili	, Member	**9.20.2016** Date Approved
Anandh Babu Pon Velayutham	, Member	**9.20/2016** Date Approved

and by **Timothy A Brusseau, Jr.** , Chair/Dean of

the Department/College/School of **Exercise and Sport Science**

and by David B. Kieda, Dean of The Graduate School.

ABSTRACT

As the identification of new targets for therapeutic intervention that might attenuate cardiovascular complications associated with type 2 diabetes are needed, our lab conducted a prior study to address that need. We reported at that time that mice treated with a potent and selective small molecule inhibitor (LB1; Lixte Biotechnology Holdings, Inc., East Setauket, NY; 1 mg/kg IP; intraperitoneal) of protein phosphatase 2A (PP2A) for the last 14 days of an obesogenic diet (12 weeks of fat-feeding) did not display vascular PP2A hyperactivation, endothelial dysfunction, or hypertension that otherwise developed in fat-fed mice treated with vehicle. We concluded that PP2A hyperactivation should be considered further as a therapeutic target for intervention. While our investigation was in progress, results from another study indicated that 2 -mg/kg LB1 IP (3 hr) evoked hyperglycemia, glucose intolerance, and hepatic glycogen depletion in chow-fed and fat-fed (3 days) rats. The authors concluded that targeting PP2A hyperactivation should not be considered as a therapeutic intervention. Based on the incongruent conclusions from these two studies, we conducted a new research study, testing the following hypotheses—that LB1 treatment for 14-days impairs: (i) peripheral glucose homeostasis; (ii) hepatic glycogen content; and (iii) insulin-mediated signal transduction in the liver. The first two hypotheses were tested using 7-week old male C57BL/6J mice who consumed standard (Con) or high fat (HF) chow for 12 weeks. Subgroups of Con and HF mice received 1 mg/kg LB1 or saline (Veh) IP for the last 14

days of testing. Glucose and insulin tolerance testing indicated that LB1 treatment does not impair peripheral glucose homeostasis in Con mice or HF mice, denying the first hypothesis. Regarding second hypothesis, LB1 treatment did not lower hepatic glycogen content, p-Akt2^{S474} / Akt2, p-Gsk3α^{S21} / Gsk3αβ, or p-GS^{S641} / GS, in lean or obese mice under basal, random-fed conditions. To test the third hypothesis, age-matched male mice that consumed standard chow were treated with LB1 or Veh for 14 days. On day 15, after a 6-hr fast, insulin or saline was administered (i.v.; intravenous) to anesthetized mice, and segments of liver were collected to assess p-Akt2^{S474} / Akt2, p-GSK3α^{S21} / GSK3α, and p-GS^{S641} / GS. Insulin-mediated signal transduction in the liver was similar regardless of LB1 treatment. We conclude that LB1 treatment in mice for 14-days does not impair: (i) peripheral glucose homeostasis; (ii) hepatic glycogen content; or (iii) insulin-mediated signal transduction in the liver.

TABLE OF CONTENTS

LIST OF FIGURES

Figures

CHAPTER 1

INTRODUCTION

Obesity, type 2 diabetes mellitus (T2DM), and insulin resistance are conditions associated with an altered endothelial cell (EC) phenotype that is, endothelial dysfunction. Eighty percent of patients with these conditions will die from cardiovascular complications. The prevalence of diagnosed and undiagnosed cases of T2DM is estimated to increase to 33% by 2050 (Boyle, Thompson, Gregg, Barker, & Williamson, 2010). Individual and societal costs will increase should this concerning projection be realized. This underscores the need to elucidate effective therapeutic targets and strategies for intervention.

1.1 Literature Review

1.1.1 Endothelial cell dysfunction

Endothelial dysfunction can be defined as attenuated arterial vasorelaxation in response to pharmacological agonists such as acetylcholine, bradykinin, or adenosine triphosphate (ATP), or physical stimuli such as increased intraluminal flow. When impaired vasorelaxation to one of these agonists is observed and the integrity of the vascular smooth muscle is verified, a strong case can be made that the endothelium is the source of the defect. Impaired endothelium-dependent vasorelaxation is an early indicator

endothelial dysfunction (Triggle & Ding, 2010). A crucial aspect of endothelial dysfunction is reduced nitric oxide (NO) bioavailability. NO bioavailability depends on a delicate balance between factors responsible for the synthesis and degradation of this molecule. In addition to contributing to vasodilation, endothelial cell derived NO has anticoagulant, anti-inflammatory, and antiproliferative properties (Alderton, Cooper, & Knowles, 2001; Sessa, 2004; Shaul, 2002). Loss of these protective mechanisms contributes importantly to the pathophysiology of micro and macrovascular diseases that characterizes obesity, T2DM, and insulin resistance (Symons, 2013; Symons & Abel, 2013; Triggle & Ding, 2010).

Progress has been made in elucidating general mechanisms that precipitate a mismatch between generation and degradation of NO that leads to cardiovascular complications such as hypertension and atherosclerosis that are associated with endothelial dysfunction. Strong evidence exists that hyperglycemia, oxidative stress, activation of the renin angiotensin system, increased proinflammatory cytokines, and lipotoxicity contribute independently and synergistically to this process (Bornfeldt & Tabas, 2011; Geraldes & King, 2010) (Figure 1). Gaining additional insight into precise mechanisms linking each of these pathways to vascular dysfunction is necessary to design and implement targeted therapeutic strategies with minimal off-target side effects. Our recent focus has concerned the contribution from lipotoxicity in general, and the lipid metabolite ceramide in particular, to lowering vascular NO production to an extent that precipitates endothelial cell dysfunction (Bharath et al., 2015; Symons et al., 2009; Symons & Abel, 2013; Wende, Symons, & Abel, 2012; Zhang et al., 2012) (Figure 2).

1.1.2 Elevated free fatty acids contribute importantly to endothelial dysfunction that is observed in obese versus lean mice

Earlier we reported that a dissociation exists between insulin mediated signal transduction in the vasculature, and impaired endothelial nitric oxide synthase (eNOS) enzyme function (Symons et al., 2009). In this regard, systemic hypertension, arterial dysfunction, and decreased basal and stimulated eNOS phosphorylation in obese mice occurred in the absence of evidence for deficient signaling via Protein kinase B (Akt) to eNOS in the vasculature (Symons et al., 2009). The apparent dissociation between vascular insulin signaling and impaired eNOS enzyme function in the context of obesity prompted an exploration into whether a component of the metabolic environment or altered signaling via another kinase to eNOS might play a role. Because fasting hyperglycemia was mild in fat-fed versus lean mice in that study, and superoxide anion (O2•-) production, nicotinamide adenine dinucleotide phosphate (NADPH)-oxidase activity, adenosine monophosphate-activated protein kinase (AMPK), and Protein Kinase A (PKA) were similar in vessels from both groups, the contribution from the three-fold elevation in free fatty acids (FFAs) in obese versus lean mice was explored more thoroughly. To do so, bovine aortic endothelial cells (BAECs) were treated with 500 uM palmitate, a concentration that lies within the physiological / pathophysiological range (Summers, 2010) and does not lead to cell death or apoptosis in response to exposures < 3 hr (Symons et al., 2009). Compared to vehicle-treated cells, palmitate impaired basal and insulin-stimulated eNOS phosphorylation at serine 1117 (p-eNOS^{S1177}) whereas extracellular signal–regulated kinases (ERK) and Akt phosphorylation was intact. Importantly, the palmitate-induced reduction of eNOS phosphorylation was sufficient to

compromise insulin-mediated NO generation by BAECs (assessed by amperometric probes), and attenuate endothelium-dependent vasorelaxation but not vascular smooth muscle function of isolated arteries (Symons et al., 2009) (assessed by isometric tension techniques). These *in vitro* results from BAECs and isolated arteries exposed to palmitate recapitulated earlier observations from arteries of obese mice in the same study, and indicate a significant component of endothelial dysfunction in obese mice is secondary to elevated FFAs.

1.1.3 The FFA metabolite ceramide contributes importantly to endothelial dysfunction that is observed in obese versus lean mice

When tissues not suited for lipid storage (e.g., skeletal muscle, liver) are exposed to increased circulating levels of FFAs, toxic bioactive lipid metabolites can accumulate and that might be associated with impaired metabolic homeostasis and increased cardiovascular risk. One such metabolite is the sphingolipid ceramide (Chun et al., 2011; Holland & Summers, 2008). Obesity and lipid exposure promote sphingolipid accumulation in peripheral tissues of rodents and humans, and ceramide accumulates in arteries from rats with uncontrolled type 2 diabetes (Wu, Song, Xu, Zhang, & Zou, 2007). Based on these reports, and our earlier findings in BAECs and isolated arteries that palmitate decreases p-eNOS^{S1177}, NO production, and endothelial but not vascular smooth muscle function (Symons et al., 2009), the specific contribution from the FFA metabolite ceramide was investigated (Zhang et al., 2012). In that study, palmitate increased de novo ceramide synthesis in BAECs, which reduced insulin and vascular endothelial cell growth factor -stimulated p-eNOS^{S1177} and p-eNOS^{S617}, eNOS dimer to

monomer formation, eNOS enzyme activity, and NO production (Zhang et al., 2012). Importantly, each effect of ceramide was negated when BAECs were incubated with palmitate concurrently with myriocin, an inhibitor of the rate limiting enzyme responsible for ceramide biosynthesis. In contrast to findings from other cell types (Holland et al., 2007), palmitate-induced ceramide accumulation in BAECs did not impair upstream signaling to eNOS from Akt, AMPK, or ERK 1/2, or increase O2•- -mediated peroxynitrite formation to an extent that compromised NO generation. In addition to BAECs, palmitate also increased endogenous ceramide biosynthesis in isolated arteries. Notably, when palmitate-induced arterial ceramide biosynthesis was prevented using pharmacological and genetic approaches, the ability of this FFA to decrease p-eNOS^{S1177} and endothelium-dependent vasorelaxation was prevented (Zhang et al., 2012). Collectively, these findings from BAECs and isolated arteries indicate that ceramide contributes importantly to palmitate-induced reductions in eNOS activation to an extent that is functionally relevant.

Next it was important to determine whether deleterious responses to ceramide accumulation observed in BAECs and isolated arteries after relatively short term (i.e., 3 hr) exposure to palmitate could be observed in a clinically relevant rodent model of obesity, T2DM, and insulin resistance (Zhang et al., 2012). As such, pharmacological and genetic approaches to limit ceramide biosynthesis in fat-fed mice were implemented to determine whether earlier findings from BAECs and isolated arteries could be recapitulated *in vivo*. Inhibition of ceramide synthesis with myriocin, or by heterozygous deletion of dihydroceramide desaturase (des1), which catalyzes de novo ceramide synthesis, prevented endothelial dysfunction and systemic hypertension, and preserved

eNOS phosphorylation in arteries from fat-fed mice (Zhang et al., 2012). Collectively, these studies support the hypothesis that arterial ceramide accumulation precipitates cellular dysfunction in part by impairing NO bioavailability.

1.1.4 Endothelial dysfunction is caused by palmitate-induced, ceramide-mediated, protein phosphatase 2A association with eNOS

After observing that palmitate and fat-feeding impair eNOS phosphorylation, NO production, and arterial vasorelaxation in a ceramide-dependent manner, our laboratory sought to elucidate the molecular mechanisms that might be responsible. Protein kinases and phosphatases respectively add and remove phosphate groups from their target proteins (Shi, 2009). Because ceramide did not alter kinase signaling to eNOS or exaggerate reactive oxygen species (ROS)-mediated destruction of eNOS (Symons et al., 2009; Zhang et al., 2012), intracellular phosphatases were examined. Protein phosphatases 1 (PP1), 2A (PP2A), and 2B (PP2B) are abundantly expressed in tissues from diabetic rats and all have potential to negatively regulate p-eNOS^{S1177} (Foulkes & Jefferson, 1984; Mehra et al., 2014; Smith, Visioli, Frei & Hagen, 2006; Wu, Song, Xu, Zhang, & Zou, 2007). While preliminary results from BAECs revealed that neither PP1 nor PP2B contributed importantly to palmitate-induced reductions in p-eNOS^{S1177} (Bharath et al., 2015), palmitate clearly activated PP2A in a ceramide-dependent manner. In this regard, palmitate-induced ceramide accumulation stimulated translocation of PP2A from the cytosolic compartment to the plasma membrane, where it colocalized with eNOS at the membrane. This colocalization between PP2A and eNOS prevented

eNOS from assembling with Akt and heat shock protein 90 (Hsp90), decreased the phosphorylation of the pool of Akt that associates directly with eNOS, and impaired full eNOS phosphorylation (Symons et al., 2009; Zhang et al., 2012). Importantly, and congruent with these findings observed in BAECs studied *in vitro*, the association between PP2A and eNOS was increased in arteries from lipid-infused and fat-fed mice in a ceramide-dependent manner (Bharath et al., 2015).

1.1.5 Ceramide activates PP2A by disrupting the interaction between inhibitor 2 of PP2A (I2PP2A) and PP2A

To this point, our results suggested strongly that FFAs in general and ceramide in particular cause PP2A activation and subsequent colocalization with eNOS. Next we focused on elucidating the mechanism whereby ceramide accumulation stimulates PP2A. In addition to ceramide and protein phosphatases that exist in the cytosol, various inhibitors of protein phosphatases are present. Mukhopadhyay et al. (2009) observed that inhibitor 2 of PP2A (I2PP2A) but not inhibitor 1 of PP2A (I1PP2A) is a major ceramide-binding protein in A549 human lung cancer cells. It was reported that when ceramide binds to I2PP2A, the tonic restraint of I2PP2A on PP2A is removed. Multiple approaches were used to determine whether this mechanism operates in BAECs when ceramide accumulates in an endogenous manner in response to palmitate. Indeed, I2PP2A and PP2A are associated in the cytosol under basal, that is, control conditions. However, when ceramide accumulates in response to palmitate exposure, it binds preferentially with I2PP2A in the cytosol. When this occurs, the I2PP2A-mediated cytosolic restraint of PP2A is removed, leading to translocation of PP2A to the plasma membrane where it

associates with membrane-bound eNOS. The effects of palmitate on the cytosolic I2PP2A:PP2A interaction were: ameliorated in palmitate-treated BAECs by pharmacological and genetic procedures that limit endogenous ceramide biosynthesis; prevented in palmitate-treated BAECs that were transfected with catalytically-inactive mutant PP2A; and recapitulated in vehicle-treated ECs after siRNA-mediated suppression of I2PP2A gene expression. Taken together, ceramide can be elevated to an extent that disrupts the restraint of I2PP2A on PP2A, PP2A colocalizes with eNOS, and eNOS enzyme activity is compromised to an extent that NO generation is impaired (Bharath et al., 2015; Symons et al., 2009; Zhang et al., 2012).

1.1.6 Ceramide-mediated PP2A activation is sufficient to evoke arterial dysfunction in obese versus lean mice

Significant rationale exists to test whether PP2A activation contributes independently to arterial dysfunction in vivo. For example, Smith et al. (2006) reported suppressed endothelial glutathione concentrations in old versus young rats activates neutral sphingomyelinases that increase vascular ceramide and PP2A activity, to thereby disrupt the balance between p-eNOS^{S1177} and p-eNOS^{T495}. Although arterial dysfunction observed in old versus young rats was reversed *in vitro* by neutral sphingomyelinase inhibition in that study, a direct effect of PP2A on arterial function was not evaluated. Wu Y et al. (2007) examined the hypothesis that PP2A-mediated dephosphorylation of p-AMPK^{T172} was responsible for impaired p-eNOS^{S1177} in vessels from mice fed a palmitate-rich versus oleate-rich high-fat diet. Interestingly, p-AMPK^{T172} and p-eNOS^{S1177} improved in vessels from mice fed palmitate-rich high-fat diet 48 hr after

retro-orbital treatment with PP2A siRNA, but the functional consequences of this biochemical modification of eNOS were not assessed. Mehra et al. (2014) reported that vascular endothelial growth factor (VEGF)-induced p-eNOS^{S1177} and NO generation were suppressed in BAECs that were coincubated with palmitate in a manner that was sensitive to ceramide biosynthesis (via myriocin) and PP2A (via okadaic acid) inhibition, confirming results reported by our laboratory using another eNOS agonist, that is, insulin (Symons et al., 2009). These authors extended their *in vitro* findings by showing growth factor induced NO production was blunted in arteries from wild-type but not serine palmitoyltransferase long chain base subunit 2 (Sptlc2) haploinsufficient mice that consumed high-fat chow for 2.5 weeks, clarifying the importance of ceramide in this regard. In all three of these studies, however, the independent contribution from PP2A activation to NO-mediated arterial function was not assessed. Earlier we used pharmacological and genetic approaches to limit arterial ceramide accumulation, and therefore vascular PP2A colocalization with eNOS, to show that ceramide contributes importantly to endothelial dysfunction and hypertension that exist in the context of diet-induced obesity (Zhang et al., 2012). Again, however, the contribution from PP2A activation *per se* was not evaluated in that study, and until recently, remained elusive.

While solid rationale exists to determine whether hyperactivation of PP2A impairs blood vessel function, concerns regarding cytotoxicity for cantharidin-derived compounds, efficacy for norcantharidin-derived compounds, and target specificity for genetic knockout models, have precluded exploration of this important question (Bonness et al., 2006; Galbo et al., 2013; Götz & Schild, 2003). Investigations of PP2A activation in the context of cancer chemotherapy using mice (Lu et al., 2009; Lu et al., 2010;

Martiniova et al., 2011) and hepatic insulin resistance using rats (Galbo et al., 2013) reported that 3-21 day treatment with the norcantharidin analogue LB1 (Lixte Biotechnology Holdings, Inc., East Setauket, NY) can be administered without pathological evidence of toxicity. LB1 is a potent and specific inhibitor of PP2A activity with relatively low activity on PP1 (Lu et al., 2009; Lu et al., 2010; Martiniova et al., 2011). We used LB1 to examine the specific contribution from PP2A to vascular dysfunction in the context of diet-induced obesity (Bharath et al., 2015).

First, we demonstrated that LB1 prevented palmitate-induced PP2A activation, restored basal and insulin-stimulated p-eNOS^{S1177} and NO production, and did not influence upstream kinase signaling to eNOS or ceramide accumulation in BAECs. Next, multiple approaches established that the PP2A – mediated disruption of Akt-Hsp90-eNOS interactions correlated with impaired p-eNOS^{S1177} and NO production, and this could be prevented by PP2A inhibition or a PP2A mutant with decreased catalytic activity. Third, after documenting that lard-oil infusion to intact mice increases vascular PP2A activity, disrupts the physical interactions among Akt-Hsp90-eNOS in the vasculature, and precipitates endothelium-dependent dysfunction, we showed that these responses could be prevented by inhibiting ceramide biosynthesis (using des1 haploinsufficient mice) or limiting PP2A activation (i.e., LB1-treated mice). Finally, dysregulation of interactions among vascular Akt-Hsp90-eNOS, endothelial dysfunction, and systemic hypertension, all were normalized when fat-fed mice were treated with LB1 but not vehicle (saline). Collectively, these findings indicate that PP2A activation evoked by palmitate in BAECs, by lard-oil infusion in mice, and by fat-feeding in mice, has deleterious consequences on endothelial function, and that pharmacological inhibition of

PP2A may reverse lipotoxicity-induced vascular dysfunction (Bharath et al., 2015).

1.1.7 Does long-term (i.e., 14 d) PP2A inhibition in mice dysregulate peripheral glucose homeostasis, impair insulin-mediated signal transduction in the liver, and lower hepatic glycogen content?

Results from our laboratory suggest strongly that therapeutic strategies targeted to lower ceramide-mediated PP2A activation might be beneficial in attenuating vascular complications associated with obesity, T2DM and insulin resistance (Bharath et al., 2015). However, while our investigation (Bharath et al., 2015) was in progress, Galbo et al. (2013) reported that PP2A hyperactivity is "unsuitable as a target for therapeutic intervention." Evidence for this statement was provided by data indicating that impaired peripheral glucose tolerance, lower hepatic glycogen content, and disrupted insulin-mediated signal transduction in the liver, exists in rats wherein PP2A was inhibited (i.e., LB1-treated) versus control rats (i.e., saline-treated). In this regard, three hours before completing a hyperinsulinemic-euglycemic clamp, male rats received 2 mg/kg LB1 or vehicle (saline) IP. Relative to vehicle-treated rats, LB1-treated animals displayed 8-10 mg/dl higher fasting plasma glucose levels and required ~ 30% less infusion of [6,6-2H] glucose to maintain plasma glucose between 100-110 mg / dl (Figure 3A). These indices of whole body insulin-resistance in LB1 versus vehicle treated rats were accompanied by marked reductions in liver glycogen content after PP2A inhibition. For example, liver glycogen content in chow-fed rats was ~ 65 versus 11 ug/mg protein in response to vehicle vs. LB1 treatment, respectively. Further, liver glycogen content in fat-fed rats was

~ 55 and 12 ug/mg protein in response to vehicle versus LB1 treatment, respectively. Therefore, LB1 markedly lowered liver glycogen to a similar extent in both chow-fed and fat-fed rats (Figure 3B).

The authors attributed lower glycogen content after PP2A inhibition (Figure 3B) to greater insulin-stimulated phosphorylation of (i) hepatic glycogen synthase (resulting in inactivation and therefore decreased glycogen synthesis) and (ii) phosphorylase (resulting in activation and therefore increased glycogen breakdown), in LB1 versus saline-treated rats.

1.2 Purpose of Study

The purpose of the present study was to determine whether 14 days x 1 mg/kg LB1 treatment in mice impairs glucose tolerance, insulin-mediated signal transduction in the liver, and hepatic glycogen content. Three hypotheses were tested.

HYPOTHESIS 1: 14 days x 1 mg / kg LB1 IP impairs peripheral glucose tolerance in mice. To test this hypothesis, historical data sets from a glucose tolerance test and an insulin tolerance test obtained from mice treated ± 1 mg/kg LB1 IP for 14 days (Bharath et al., 2015) were reanalyzed.

HYPOTHESIS 2: 14 days x 1 mg / kg LB1 IP treatment lowers hepatic glycogen content. To test this hypothesis, historical liver samples from mice treated ± 1 mg/kg LB1 for 14 days (Bharath et al., 2015) were analyzed for glycogen content, p-Akt2^{S474} / Akt2, p-Gsk3α^{S21} / Gsk3αβ, and p-GS^{S641} / GS.

HYPOTHESIS 3: 14 days x 1 mg / kg LB1 treatment impairs insulin-stimulated signal transduction in the liver. To test this hypothesis, mice that were treated for 14 days

with LB1 or vehicle IP received insulin or vehicle-stimulation i.v. Five minutes later, liver segments were collected, and immunoblotting was used to assess p-Akt2^{S474} / Akt2, p-Gsk3α^{S21} / Gsk3α, and p-GS^{S641} / GS.

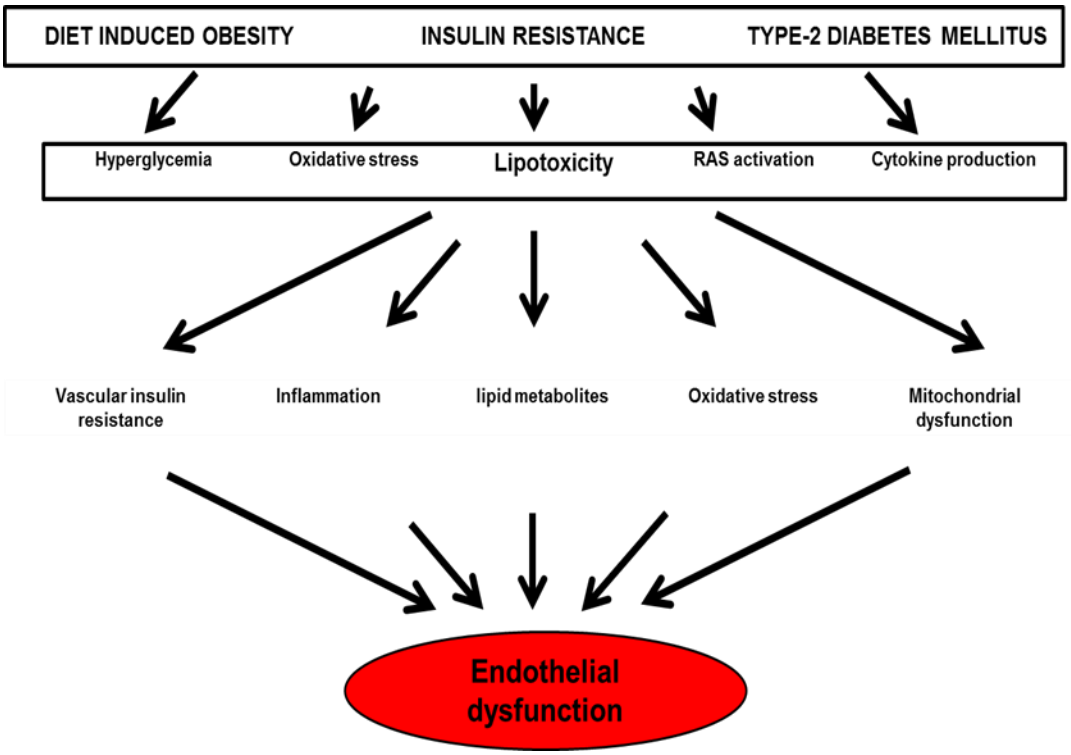

Figure 1 Multiple mechanisms contribute to endothelial dysfunction that exists in subjects with diet-induced obesity, insulin resistance, and type 2 diabetes mellitus. Of these, lipotoxicity can decrease endothelial function by: (i) impairing agonist-induced signaling to eNOS in endothelial cells and blood vessels; (ii) increasing inflammation; (iii) stimulating accrual of toxic sphingolipids, for example, ceramide; (iv) promoting oxidative stress to an extent that overwhelms the antioxidant environment; and/or by (v) potentially precipitating mitochondrial dysfunction (Wende, Symons, & Abel, 2012).

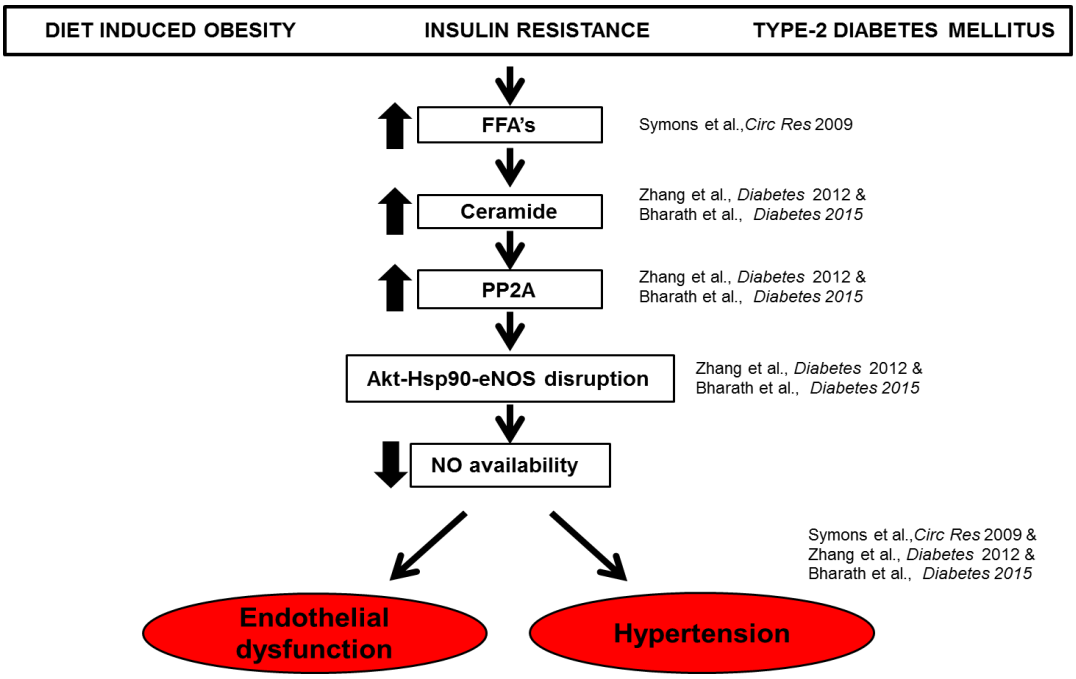

Figure 2 DIO elevates FFAs to an extent that increases vascular ceramide accumulation. Ceramide binds I2PP2A in the cytosol, and relieves the restraint of I2PP2A on PP2A. PP2A translocates from cytosol to membrane, binds eNOS, and disrupt the Akt-Hsp90-eNOS interaction to an extent that impairs NO generation, leading to endothelial dysfunction and hypertension.

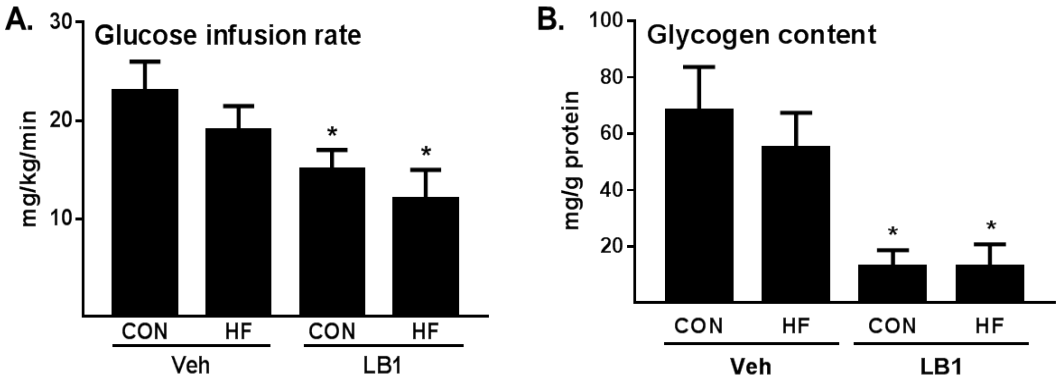

Figure 3 Rats consumed chow (Con) or high fat (HF) diet for 3 days. Three hours prior to a hyperinsulinemic-euglycemic clamp rats were treated with vehicle (Veh) or LB1. (A) A lower glucose infusion rate was required to maintain euglycemia in LB1 versus Veh-treated rats, regardless of diet. (B) Segments of liver were obtained immediately following the hyperinsulinemic-euglycemic clamp. Liver glycogen content was lower in LB1 versus Veh-treated rats, regardless of diet. Results are mean ± *SEM*. **P* <0.05 LB1 versus Veh for CON and HF (Galbo et al., 2013).

CHAPTER 2

MATERIALS AND METHODS

2.1 Cohort 1

2.1.1 Animals

All protocols were approved by the University of Utah (UU) Institutional Animal Care and Use Committee (IACUC; 13-06004). Mice were maintained in a temperature-controlled barrier facility with a 12-hr light/dark cycle and were given free access to food and water. Seven-week old male C57BL/6J mice (n =24) were obtained from the Jackson Laboratory (Bar Harbor, ME) and consumed standard rodent chow (D12450B, Research Diets, Inc., New Brunswick, NJ) containing (kcal) 10% fat, 70% carbohydrate, and 20% protein (control diet; CON) during a one-week quarantine period. Next, mice either continued the CON diet or were placed on high fat chow (D12451, Research Diets, Inc., New Brunswick, NJ) containing (kcal) 45% fat, 35% carbohydrate, and 20% protein for 12 weeks [high fat (HF) diet] (Bharath et al., 2015; Symons et al., 2009; Zhang et al., 2012). For the final 14 days, subgroups of CON and HF mice received vehicle (saline) or LB1 (1 mg/kg/day) (Bharath et al., 2015; Lu et al., 2009; Lu et al., 2010; Martiniova et al., 2011). Next, mice completed a glucose tolerance test (GTT) and insulin tolerance test (ITT; described below). At least 48 hr following the GTT or ITT, mice were anesthetized with 2-5% isoflurane, the chest was opened, the heart removed, and liver samples were

excised and placed in eppendorf tubes, frozen in liquid nitrogen, and stored at -80ºC. Segments of liver were used for immunoblotting and to quantify glycogen content.

2.1.2 Glucose Tolerance Test (GTT)

Mice were made to fast for 6 hr by removal to a clean cage without food at the end of their dark (feeding) cycle, that is, 6:00 AM. After 6 hr, mice were weighed, and blood glucose was determined using a glucometer (Onetouch Ultra2; Life Scan, Inc., Milpitas, CA) via a tail clip (i.e., 0-min). Next, glucose (1 mg/g, IP) was administered to conscious animals and blood glucose determined after 5, 15, 30, 60, and 120-min. At 0-min, an extra volume of blood (~50ul) was obtained. Samples were centrifuged for 10 min x 3000 rpm at 4°C to assess serum insulin (ELISA, Linco, Billerica, MA) and free fatty acids (FFAs; colorimetric, half-micro test, Roche Diagnostics, Indianapolis, IN) (Bharath et al., 2015; Symons et al., 2009; Zhang et al., 2012). Results were used to calculate the homeostasis model assessment of insulin resistance (HOMA-IR), that is, fasting glucose (mmol/L) × fasting serum insulin (mU/L) divided by 22.5 (Matthews, et al., 1985). Blood glucose at each time point during the GTT, and the calculated HOMA-IR, was compared between Con-Veh and Con-LB1 mice, and HF-Veh and HF-LB1 mice.

2.1.3 Insulin Tolerance Test (ITT)

Mice were made to fast for 4 hr by removal to a clean cage at the end of their dark (feeding) cycle. After 4 hr, mice were weighed, a blood sample was obtained via tail clip (i.e., 0-min), and glucose was measured using a glucometer (Onetouch Ultra2; Life Scan, Inc., Milpitas, CA). Next, insulin (Humulin, Eli Lilly, Indianapolis, IN) was injected

(0.75 U/kg body weight; IP), and blood glucose was assessed via tail clip 5, 15, 20, 25, and 30- min later (Bharath et al., 2015; Symons et al., 2009; Zhang et al., 2012). Blood glucose at each time point was compared between Con-Veh and Con-LB1 mice, and HF-Veh and HF-LB1 mice.

2.1.4 Glycogen content

Segments of liver were obtained from Con-Veh, Con-LB1, HF-Veh, and HF-LB1 mice (Bharath et al., 2015). Liver glycogen content was measured using a commercially available kit (Cayman Chemical, Ann Arbor, Michigan) according to the manufacturer's instructions (Kim, Kim, & Park, 2012). In brief, 300 mg of minced liver tissue was combined with 2 ml of Halt protease and phosphatase inhibitor cocktail (Thermo Scientific, Rockford, IL). After homogenization and sonication on ice, samples were centrifuged for 10 min x 3000 rpm at 4°C. Aliquots of supernatant were diluted 1:10 – 1:100, depending on the protein concentration obtained, and glycogen was assessed.

2.1.5 Immunoblotting

Segments of liver were obtained from Con-Veh, Con-LB1, HF-Veh, and HF-LB1 mice that were used to assess GTT and ITT. (Bharath et al., 2015) Liver tissue was homogenized in ice-cold homogenization cell lysis buffer pH 7.2-7.4 (0.01 M Hepes, 0.05 M sodium fluoride, 0.002 M EDTA, 0.05M Disodium pyrophosphate, 0.15M sodium chloride, 0.02M Tris-HCl ,1% Triton X-100), with Halt protease and phosphatase inhibitor cocktail (Thermo Scientific, Rockford, IL). Tissues were sonicated on ice and the resulting homogenate was centrifuged for 20 min at 13,000 rpm at 4°C. Aliquots of

supernatant were stored at −80°C for later immunoblotting and protein analyses (Bharath et al., 2015; Symons et al., 2009; Zhang et al., 2012).

Protein concentration for immunoblotting was determined using a Pierce™ BCA Protein Assay Kit (Thermo Scientific, Rockford, IL). Western Blotting was used to detect specific proteins in each tissue sample. Proteins were separated by the length of the polypeptide using gel electrophoresis. Protein phosphorylation was determined using western blot procedures. Equal amounts of protein were suspended in loading buffer containing Tris-Glycine SDS (Novex, Life Tech, Carlsbad, CA), incubated for 5 min in a 37°C water bath, and 14.4 mM 2-mercaptoethanol was added. Resolved proteins in sodium dodecyl sulfate polyacrylamide gel electrophoresis (SDS-PAGE) were transferred to a polyvinylidene difluoride (PVDF) membrane (Millipore Immobilon-P Transfer membrane; Millipore Corp., Billerica, MA) for overnight incubation at 4°C. Following the transfer, membranes were blocked with 5% bovine serum albumin (BSA) in Tris-buffered saline with 1% Tween-20 (TBST) for 45 min at room temperature. Blocked membranes then incubated with the respective primary antibody for phosphorylated proteins overnight at 4°C. Next, membranes were washed with TBST (3× 15 min), and incubated with the appropriate secondary antibody conjugated to horseradish peroxidase-conjugated antirabbit IgG (Rockland, Limerick, PA) or antimouse IgG (Rockland, Limerick, PA) for 1 hour at room temperature. Membranes were washed with TBST (4 × 5 min) and scanned (Licor Odyssey scanner) (Bharath et al., 2015; Symons et al., 2009; Zhang et al., 2012; Zhang et al., 2009). Dilution conditions were: 1: 1000, 5% BSA/TBST, 10% gel for p-Akt2^{S474}, AKT2, p-GSK3α^{S21}, p-GS^{S641}, GS, GAPDH (Cell Signaling Technology, Danvers, MA) and Gsk3αβ (Santa Cruz Biotechnology, Santa

Cruz, CA) (Bharath et al., 2015; Symons et al., 2009; Zhang et al., 2012; Zhang et al., 2009).

2.2 Cohort 2

2.2.1 Animals

All protocols were approved by UU IACUC protocol # 13-06004. 17-week-old male C57BL/6J mice (n =20) were familiarized for 1 week, injected with vehicle (saline; n =10) or LB1 (1 mg/kg/day; n =10; IP) for 14 consecutive days (Bharath et al., 2015), and weighed daily. Next, (i) body composition was assessed using nuclear magnetic resonance imaging (NMR) (Bharath et al., 2015) and compared between vehicle-treated (n =10) and LB1-treated (n =10) mice, (ii) random-fed and 14 hr fasted blood glucose measurements were collected via tail clip procedures (Bharath et al., 2015; Symons et al., 2009; Zhang et al., 2012) and compared between vehicle-treated (n =10) and LB1-treated (n =10) mice, and (iii) liver samples were obtained from anesthetized, vehicle-treated mice following i.v., saline (n =5) or insulin (n =5) administration, and LB1-treated mice following i.v., saline (n =5) or insulin (n =5) administration. Details are provided below.

2.2.2 Body composition

Lean mass, fat mass, and fluid mass were assessed in conscious mice via NMR (Bruker Minispec Model Mq series 7.5; Bruker Optics, Inc., Billerica, MA) after 14 consecutive days of vehicle or LB1 treatment (Bharath et al., 2015).

2.2.3 Insulin-mediated signal transduction

Mice were treated for 14 consecutive days with vehicle or LB1. On day 15, after a 6-hr fast, mice were anesthetized using 2-5% isoflurane. When an appropriate plane of anesthesia was achieved, the chest was opened and insulin (Humulin 3.3mU / g body weight) or vehicle (saline) was administered i.v (Zhu et al., 2013). Five minutes later, the heart was excised and segments of liver were collected to assess p-Akt2^{S474} / Akt2, p-GSK3α^{S21} / GSK3α, and p-GS^{S641} / GS, (Cell Signaling Technology, Danvers, MA). Each endpoint was assessed in four groups, that is, vehicle-treated mice ± insulin and LB1-treated mice ± insulin (n =5 each) (Symons et al., 2009; Zhu et al., 2013).

2.2.4 Immunoblotting

Segments of liver were prepared and processed for immunoblotting as we described earlier (Bharath et al., 2015; Symons et al., 2009; Zhang et al., 2012; Zhang et al., 2009)

2.3 Statistical Analyses

Data are presented as mean ± standard error of the mean (SEM). Comparison of one endpoint (e.g., lean mass) between groups (e.g., vehicle-treated vs. LB1 treated mice) was made using an unpaired t test. Comparison of multiple time-points (e.g., blood glucose at 0, 5, 15, 30, 60, and 120-min) between two groups (e.g., vehicle-treated and LB1 treated mice) was assessed using a two-way repeated measures analysis of variance. Comparison of one endpoint (e.g., liver p-GS^{S641}) among four groups (e.g., Veh-saline, Veh-insulin, LB1-saline, LB1-insulin) was made using a one-way analysis of variance. Significance was accepted when $P < 0.05$. Tukey post hoc tests were performed when

significant main effects were obtained. Statistics were performed using GraphPad Prism version 7.

To determine the fold change from Con-Veh mice regarding the measured endpoints (i.e., hepatic glycogen content, p-Akt2^{S474} / Akt2, p-Gsk3α ^{S21} / Gsk3αβ, and p-GS^{S641} / GS) observed in Con-LB1, HF-Veh, and HF-LB1 animals (Hypotheses 1 and 2), the following approach was used. p-Akt2^{S474} / total Akt2 is used as an example. The densitometric ratios for p-Akt2^{S474} / Akt2 were determined for all mice within the Con-Veh group. The group mean average was calculated and normalized to 1.0, by dividing each ratio by the group mean value. Next, the ratio of p-Akt2^{S474} / Akt2 was determined for samples representing the other groups (i.e., Con-LB1, HF-Veh, and HF-LB1). Each of these values was divided by the group mean p-Akt2^{S474} / Akt2 obtained from the Con-Veh group, and expressed as fold-change relative to Con-Veh (Bharath et al., 2015; Symons et al., 2009; Zhang et al., 2012; Zhang et al., 2009).

To determine the fold change from SAL-Veh mice regarding the measured endpoints (i.e., p-Akt2^{S474} / Akt2, p-Gsk3α ^{S21} / Gsk3αβ, and p-GS^{S641} / GS) observed in SAL-ins, LB1-Veh, and LB1-ins animals (Hypothesis 3), the following approach was used. p-Akt2^{S474} / total Akt2 is used as an example. The densitometric ratios for p-Akt2^{S474} / Akt2 were determined for all mice within the SAL-Veh group. The group mean average was calculated and normalized to 1.0, by dividing each ratio by the group mean value. Next, the ratio of p-Akt2^{S474} / Akt2 was determined for samples representing the other groups (i.e., SAL-ins, LB1-Veh, and LB1-ins). Each of these values was divided by the group mean p-Akt2^{S474} / Akt2 obtained from the SAL-Veh group, and expressed as fold-change

relative to SAL-Veh group (Bharath et al., 2015; Symons et al., 2009; Zhang et al., 2012; Zhang et al., 2009).

CHAPTER 3

RESULTS

3.1 Peripheral Glucose Homeostasis

3.1.1 Glucose Tolerance Test (GTT)

The purpose of this experiment was to test the hypothesis that 14 days of LB1 treatment impairs peripheral glucose tolerance in lean and obese mice. No differences in blood glucose between CON-Veh and CON-LB1 mice were obtained at any time point during the GTT (Figure 4A). Blood glucose was lower (p <0.05) in HF-LB1 versus HF-Veh mice at 60 and 120 min of the GTT (Figure 4B).

Fasting blood glucose (mg / dl), that is, the "0" time point, was similar in CON-Veh (117 ± 11) versus CON-LB1 (111 ± 13) mice, and in HF-Veh (133 ± 4) versus HF-LB1 (127 ± 18) mice. Fasting serum insulin (ng/ml) that is, the "0" time point, was similar in CON-Veh (0.59 ± 0.06) versus CON-LB1 (0.46 ± 0.04) mice, and was lower (p <0.05) in HF-LB1 (0.35 ± 0.01) versus HF-Veh (0.68 ± 0.04) mice. HOMA-IR, calculated using fasting glucose and insulin, was similar between CON-Veh (4.42 ± 0.70) and CON-LB1 (3.19 ± 0.59) mice, but was lower (p <0.05) in HF-LB1 (2.75 ± 0.42) versus HF-Veh (5.56 ± 0.45) mice (Figure 4C). Taken together, these results do not support the original hypothesis.

3.1.2 Insulin Tolerance Test (ITT)

The purpose of this experiment was to test the hypothesis that 14 days of LB1 treatment impairs peripheral sensitivity to insulin in lean and obese mice. Fasting blood glucose (mg / dl), that is, the "0" time point, was lower (p <0.05) in CON-LB1 (76 ± 4) versus CON-Veh (99 ± 6) mice, and in HF-LB1 (70 ± 5) versus HF-Veh (110 ± 6) mice. Blood glucose was lower (p <0.05) at 5, 10, 15 and 20-min following insulin administration in CON-LB1 versus CON-Veh mice (Figure 5A). Likewise, blood glucose was lower (p <0.05) in HF-LB1 versus HF-Veh mice 5,10, 20, and 25-min following insulin administration (Figure 5B).

To control for differences in fasting blood glucose that existed between lean and obese mice treated with Veh (Figure 5A) and LB1 (Figure 5B), the "0" time point blood glucose for all mice was converted to 100%, and insulin-mediated changes in circulating blood glucose in the respective groups was expressed relative to 100%. Blood glucose was lower (p <0.05) at 5 and 20 min following insulin administration in CON-LB1 versus CON-Veh mice (Figure 5C). Likewise, blood glucose was lower (p <0.05) in HF-LB1 versus HF-Veh mice 20 min following insulin administration (Figure 5D). Together, these data do not support the original hypothesis.

3.2 Hepatic Glycogen Content

3.2.1 Glycogen content in liver

The purpose of this experiment was to test the hypothesis that 14 days of LB1 treatment lowers liver glycogen content in mice. No differences existed among groups concerning liver glycogen content (Figure 6). These results do not support the original

hypothesis.

3.2.2 Basal p-Akt2 ^{S474}, p-Gsk3α ^{S21}, and p-GS ^{S641} in liver

The purpose of this experiment was to test the hypothesis that 14 days of LB1 treatment increases hepatic p-Akt2^{S474} / Akt2, p-Gsk3α ^{S21} / Gsk3αβ, and p-GS^{S641} / GS in mice. No changes were observed among groups concerning these endpoints (Figures 7A-7C). Together, these results do not support the original hypothesis.

3.3 Insulin-Mediated Signal Transduction in Liver

3.3.1 Basal and insulin-stimulated p-Akt2 ^{S474}, p-Gsk3α ^{S21}, and p-GS ^{S641} in liver

The purpose of this experiment was to test the hypothesis that 14 days of LB1 treatment impairs insulin-stimulated p-Akt2^{S474} / Akt2, p-Gsk3α^{S21} / Gsk3α, and p-GS^{S641} / GS in the liver. Fourteen days of LB1 treatment did not alter body mass (Figure 8A), body composition (Figure 8B,C), or random-fed blood glucose (Figure 8D). On Day 15, fasting blood glucose was lower (p <0.05) in LB1 versus Veh-treated mice (Figure 8D). To assess insulin-mediated signal transduction in the liver, vehicle-treated mice received i.v. saline (n =5) or insulin (n =5), and LB1-treated mice received i.v. saline (n =5) or insulin (n =5). Compared to vehicle-treated mice given saline, insulin increased (p <0.05) p-Akt2^{S474} / Akt2, but neither p-Gsk3α^{S21} / Gsk3α nor p-GS^{S641} / GS were altered. Compared to LB1-treated mice given saline, insulin increased (p <0.05) p-Akt2^{S474} / Akt2, but neither p-Gsk3α^{S21} / Gsk3α nor p-GS^{S641} / GS were altered (Figure 9A-9C). The ability of insulin versus saline to increase p-Akt2^{S474} / Akt2 in the liver was similar

between Veh-treated 5.6±1.22-fold and LB1-treated 3.4±0.37-fold mice. Taken together, results concerning insulin-mediated p-Akt2^{S474} / Akt2, p-Gsk3α^{S21} / Gsk3α, and p-GS^{S641} / GS were similar between Veh-treated and LB1-treated mice.

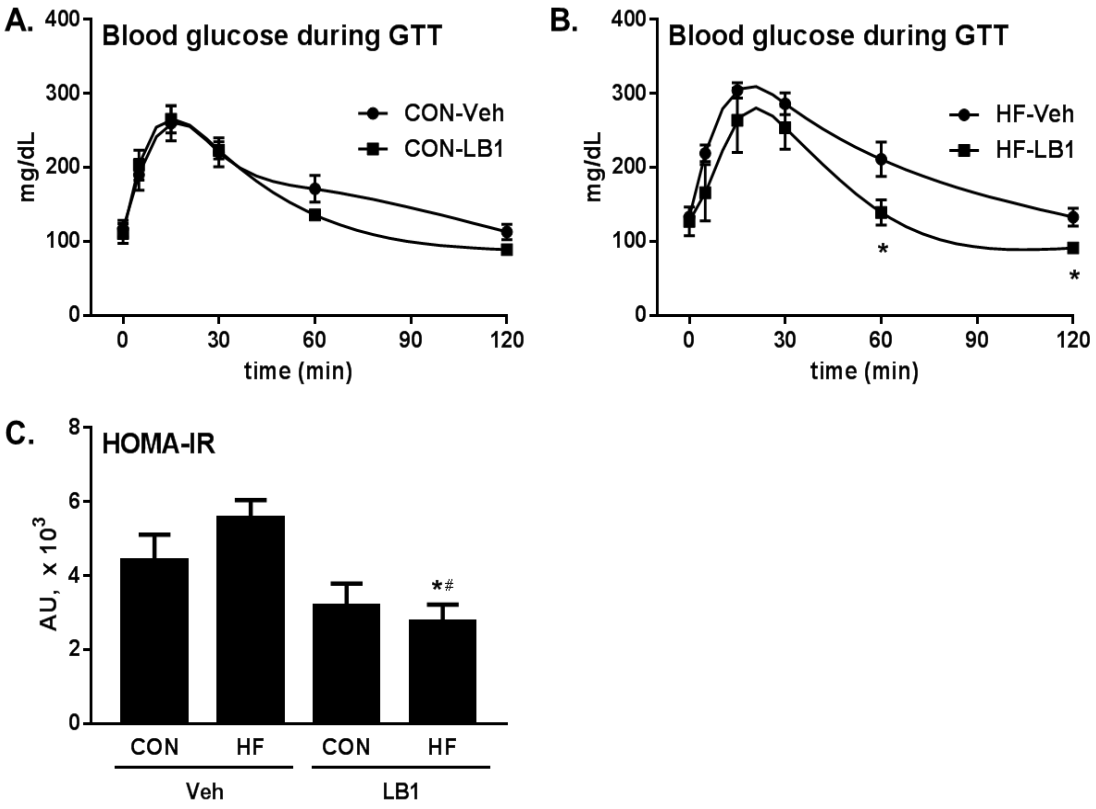

Figure 4 Blood glucose during the glucose tolerance test (GTT). Blood glucose was similar in lean mice regardless of LB1 treatment (A). Blood glucose was lower (p <0.05) in obese mice treated with saline versus LB1 at 60 and 120 min (B). HOMA-IR was similar in lean mice regardless of LB1 treatment, whereas HOMA-IR was lower (p <0.05) in obese mice treated with LB1 versus. Veh. (C). CON, mice that consumed standard chow; HF, mice that consumed high fat chow, n =6-8 mice per group. Veh, vehicle i.e., saline; LB1, PP2A inhibitor. Results represent mean ± *SEM*. *P < 0.05 versus Con-Veh; #P < 0.05 versus HF-Veh.

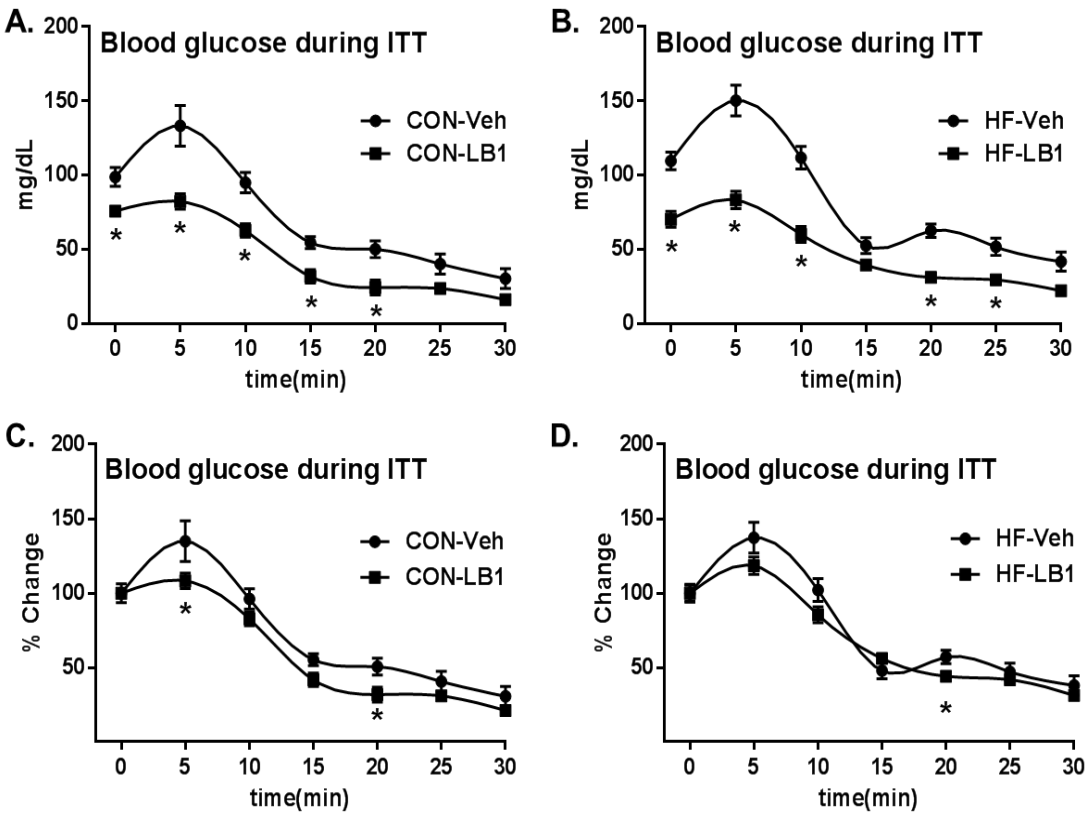

Figure 5 Blood glucose during the insulin tolerance test (ITT). Blood glucose was lower (p <0.05) before (i.e., 0-min) and 5, 10, 15 and 20-min postinsulin administration in CON-LB1 versus CON-Veh mice (A). Blood glucose was lower (p <0.05) before (i.e., 0-min) and 5, 10, 20, and 25-min postinsulin administration in HF-LB1 versus HF-Veh mice (B). Blood glucose was lower (p <0.05) at 5 and 20 min postinsulin administration in CON-LB1 versus CON-Veh mice (C). Blood glucose was lower (p <0.05) at 20-min postinsulin administration in HF-LB1 versus HF-Veh mice (D). CON, mice that consumed standard chow; HF, mice that consumed high fat chow, n =5-7 mice per group. Veh, vehicle, that is, saline; LB1, PP2A inhibitor. Results represent mean ± *SEM*. *P < 0.05 versus respective Veh-treated group.

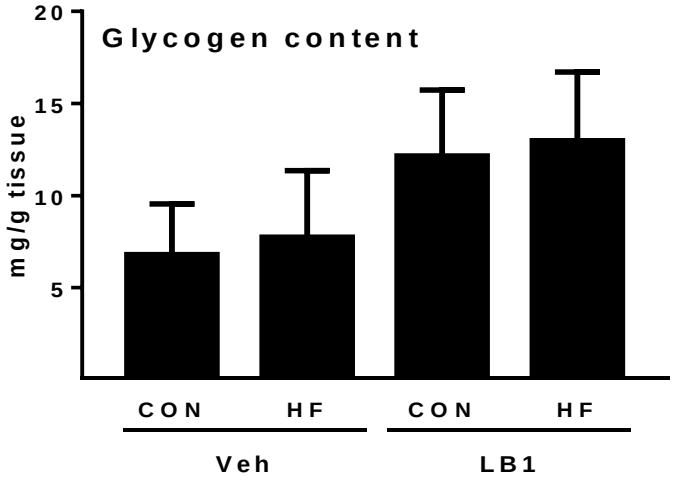

Figure 6 Liver glycogen content. No differences among groups were observed regarding liver glycogen content. CON, mice that consumed standard chow; HF, mice that consumed high fat chow. Veh, vehicle, that is, saline; LB1, PP2A inhibitor. Results represent mean ± *SEM*, *n* =6-8 mice per group.

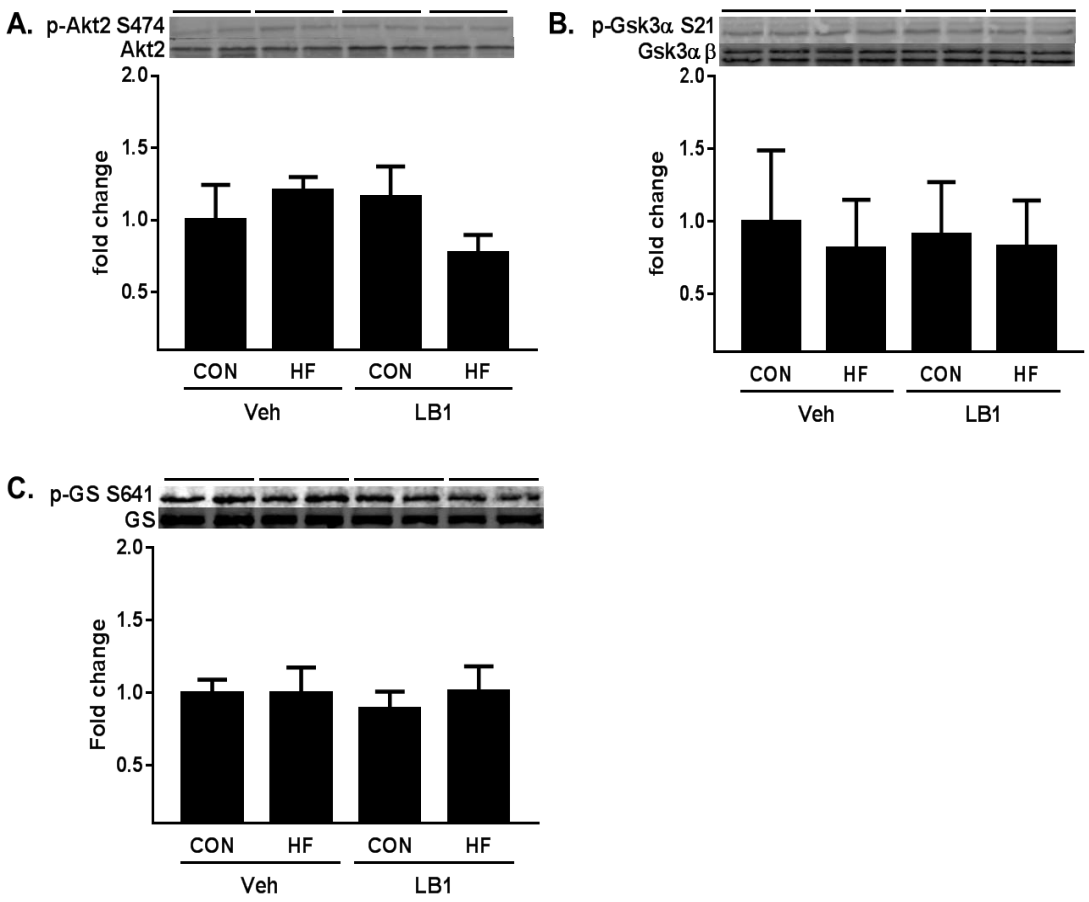

Figure 7 Kinase regulation of hepatic glycogen content. Basal p-Akt2^{S474} / Akt2, p-Gsk3αβ^{S21} / Gsk3α, and p-GS^{S641} / GS were similar in lean and obese mice regardless of LB1 treatment. Results represent mean ± *SEM*, *n* =5-6 mice per group.

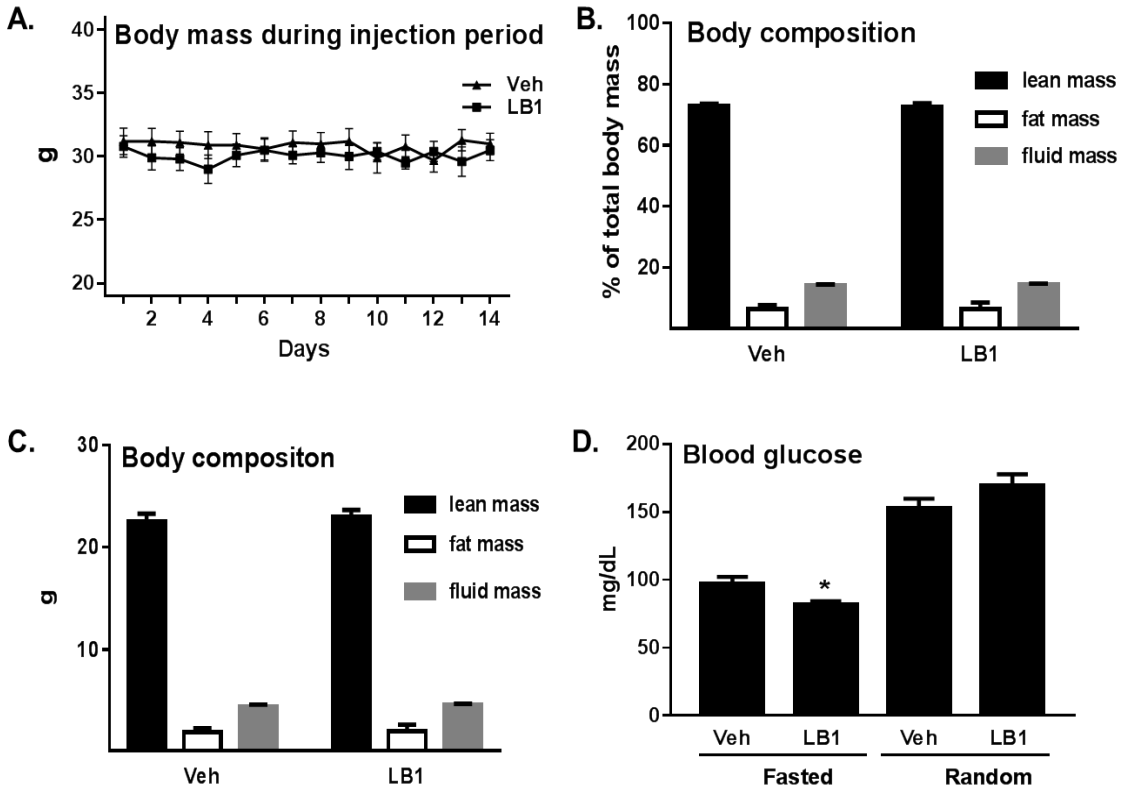

Figure 8 Body mass, body composition, and blood glucose. PP2A inhibition via LB1 treatment for 14 days does not alter body mass (A), body composition (B, C), or random-fed blood glucose (D). However, fasted blood glucose was lower in LB1 versus Veh-treated mice. Veh; vehicle (saline) treatment. Results represent mean ± *SEM*. n =10 mice per group.*$P < 0.05$ versus Veh.

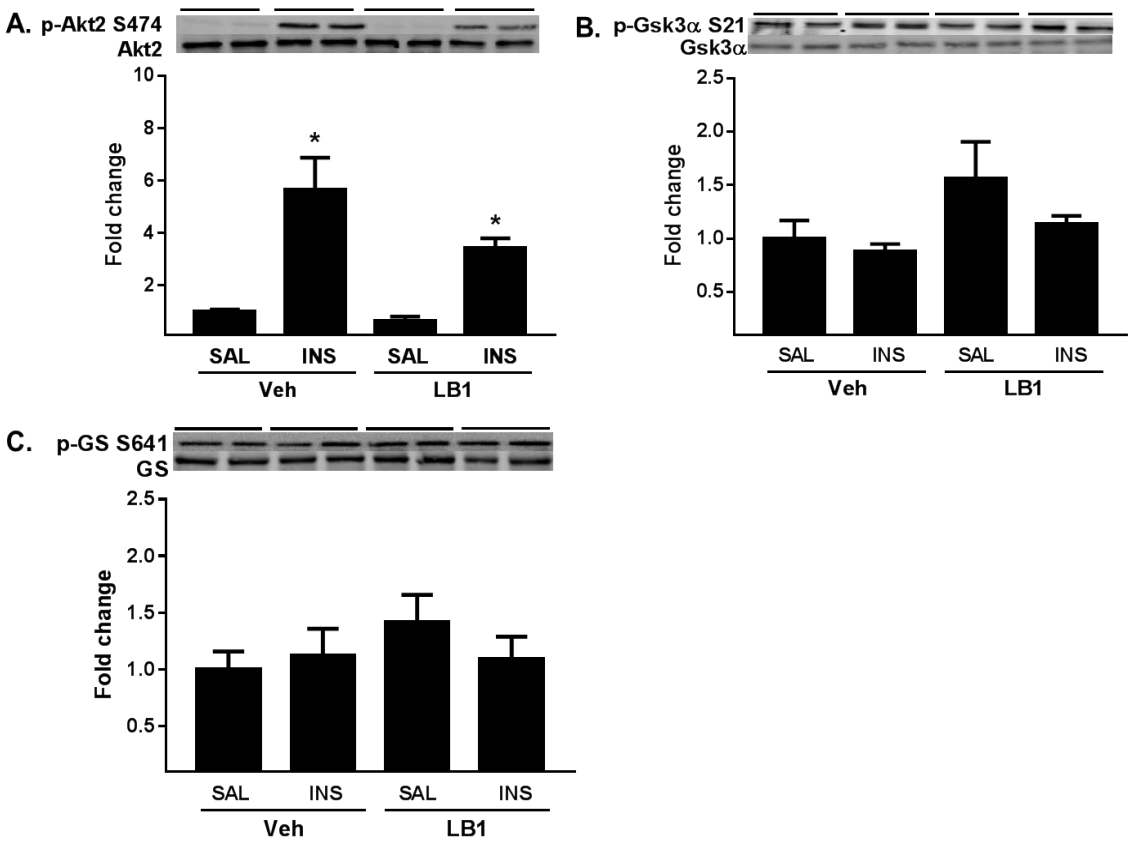

Figure 9 Insulin-mediated signal transduction. Ins (insulin) increased (p <0.05) hepatic p-Akt2^{S474} / Akt2 regardless of LB1 treatment. Neither p-Gsk3α^{S21} / Gsk3α nor p-GS^{S641}/ GS were increased by insulin. Results represent mean ± *SEM*, n =4-5 mice per group. *P < 0.05 versus respective SAL.

CHAPTER 4

DISCUSSION

4.1 Summary of Main Findings

Identifying new targets for therapeutic intervention that might attenuate cardiovascular complications associated with type 2 diabetes is needed. In an earlier report we showed that mice treated with a potent and selective small molecule inhibitor (LB1; Lixte Biotechnology Holdings, Inc., East Setauket, NY; 1 mg/kg IP) of protein phosphatase 2A (PP2A) for the last 14 days of an obesogenic diet (12 weeks of fat-feeding) did not display vascular PP2A hyperactivation, endothelial dysfunction, or hypertension that otherwise developed in fat-fed mice treated with vehicle (Bharath et al., 2015). These results provide strong proof of concept that PP2A inhibition should be considered further as a target for intervention in the context of lipotoxicity-induced cardiovascular complications. Conversely, findings from another laboratory indicated that LB1 evokes hyperglycemia, glucose intolerance, and hepatic glycogen depletion in rats, and the authors concluded that targeting PP2A hyperactivation should not be considered as a therapeutic intervention (Galbo et al., 2013). Important differences between the two investigations exist, for example, species studied, fat-feeding protocol, LB1 dose, and/or LB1 duration of treatment. The purpose of this study was to determine whether LB1 treatment for 14-days impairs: (i) peripheral glucose homeostasis; (ii) hepatic glycogen

content; and (iii) insulin-mediated signal transduction in the liver of mice. Our results indicate that 1 mg/kg LB1 IP x 14 days attenuates vascular PP2A activity, but does not adversely affect circulating blood glucose, the ability of mice to clear a glucose load, or insulin-mediated signal transduction in the liver. As such, we believe that further research into the effectiveness and practicality of PP2A inhibition in cardiovascular pathologies related to PP2A hyperactivation is warranted.

4.2 Peripheral Glucose Homeostasis

Insulin stimulates glycogen synthesis by phosphorylation (activation) of Akt, which phosphorylates (inactivates) Gsk3α. Since Gsk3α phosphorylates (inactivates) glycogen synthase (GS), the result of insulin-mediated Akt phosphorylation is increased GS activity and glycogen synthesis. This process is impaired in the context of insulin resistance associated with type 2 diabetes mellitus, at least, in part, at the level of Akt phosphorylation. While Akt can be stimulated by insulin-receptor mediated activation, it is concurrently under negative control by phosphatases, particularly PP2A. Because lipotoxicity increases PP2A activity, it is reasonable to hypothesize that heightened PP2A activity might contribute to decreased Akt phosphorylation in the context of insulin resistance. Galbo et al. (2013) sought to determine whether PP2A inhibition has therapeutic applications in this regard. Indeed, the authors demonstrated that 3 hr x 2 mg/kg LB1, a PP2A inhibitor, increased liver p-Akt2 by ~ 35% in a well-accepted model of hepatic insulin resistance, that is, rats fed high-fat chow for 3 days. Using this model, the authors investigated whether improved hepatic insulin signaling might enhance insulin sensitivity. To do so, three hours before completing a hyperinsulinemic-

euglycemic clamp, rats received 2 mg/kg LB1 or vehicle (saline) IP. Contrary to their hypothesis, LB1-treated animals displayed 8-10 mg/dl higher fasting plasma glucose levels, and required ~ 30% less infusion of [6,6-2H] glucose to maintain plasma glucose between 100-110 mg / dl, versus vehicle-treated rats. To determine if relatively long term LB1 treatment with a lower yet efficacious dose of LB1 recapitulates these deleterious findings in mice, we performed glucose and insulin tolerance testing in lean and obese mice treated for the last 14 days of a 12-week protocol with 1 mg/kg LB1 or vehicle. Contrary to our hypothesis, which was based on results from Galbo et al. (2013), results from a glucose tolerance test and insulin tolerance indicated that LB1 treatment does not adversely affect the ability of lean or obese mice to process a glucose or insulin load, when compared to findings from lean and obese mice treated with saline. In fact, under fasting conditions, and at several time points during the GTT and ITT, blood glucose was lower in LB1 versus saline-treated mice.

4.3 Hepatic Glycogen Content and Insulin-Mediated Signal Transduction in the Liver

Insulin stimulates phosphorylation (activation) of Akt which leads to phosphorylation (inactivation) of Gsk3α. Because Gsk3α normally phosphorylates (inhibits) glycogen synthase, the end result of insulin stimulation is glycogen synthesis. Galbo et al. (2013) showed that LB1 treatment markedly lowers liver glycogen content in lean and obese rats, despite the fact that PP2A inhibition increased insulin-stimulated p-Akt2 and p-Gsk3α. A further exploration of mechanisms in that study revealed that PP2A inhibition precipitated greater insulin-stimulated phosphorylation of: (i) hepatic glycogen synthase

(resulting in inactivation and therefore decreased glycogen synthesis) and (ii) phosphorylase (resulting in activation and therefore increased glycogen breakdown). To investigate this in the context of our experimental conditions, liver glycogen content was quantified in lean and obese mice treated with LB1 or vehicle for 14 consecutive days. No differences were observed among groups. Because we originally hypothesized that liver glycogen content would be lower in LB1 versus vehicle-treated mice regardless of diet, we examined several nodes in the insulin-mediated signaling pathway under basal conditions that previously had been implicated by Galbo et al (2013). Congruent with our findings concerning hepatic glycogen content and peripheral glucose homeostasis, yet contrary to results presented by Galbo et al. (2013), we observed that basal p-Akt2^{S474} / Akt2, p-Gsk3α ^{S21} / Gsk3αβ, and p-GS^{S641} / GS were similar in liver obtained from lean and obese mice regardless of LB1 treatment. While these results suggest that insulin-mediated signal transduction is not altered by LB1 treatment in the context of our experimental conditions under basal conditions, it is not unreasonable to hypothesize that the situation could be different in response to acute insulin stimulation. We investigated this possibility in a separate cohort of mice. Specifically, vehicle-treated mice received acute administration of saline or insulin i.v., and LB1-treated mice received acute administration of saline or insulin i.v. Compared to mice given saline, insulin increased p-Akt2^{S474} / Akt2 to the same extent in lean and obese mice regardless of LB1 treatment, whereas neither p-Gsk3α^{S21} / Gsk3α nor p-GS^{S641} / GS were altered. Collectively, a 14 day regimen of 1 mg/kg LB1 does not alter hepatic glycogen content under basal conditions, or p-Akt2^{S474} / Akt2, p-Gsk3α^{S21} / Gsk3α, or p-GS^{S641} / GS under basal or insulin-stimulated conditions.

Several reasonable explanations exist for why 2 mg/kg LB1 x 3 hr might have deleterious consequences concerning peripheral glucose homeostasis, hepatic glycogen content, and insulin-mediated signal transduction in rats, whereas 1 mg/kg LB1 x 14 days might not evoke adverse consequences. These explanations include the: (i) species studied (rats vs. mice); (ii) dose / duration of LB1 treatment (2 mg/kg x 3 hr vs. 1 mg/kg x 14 days); (iii) methods to assess peripheral glucose homeostasis (hyperinsulinemic-euglycemic clamp vs. glucose tolerance test and insulin tolerance test); (iv) procedures to evaluate insulin-mediated signal transduction (4 mU/kg/min insulin x 20 min in conscious rats vs. 3.3mU / g body weight i.v. in anesthetized mice).

4.4 Conclusion

In conclusion, we report that PP2A inhibition is not associated with impaired peripheral glucose, hepatic glycogen content, and insulin-mediated signal transduction in the liver. Therefore, our results suggest that PP2A hyperactivation should be considered further as a therapeutic target for intervention, and that lowering PP2A activation might be beneficial in the obesity, type 2 diabetes, and insulin resistance.

REFERENCES

Alderton, W. K., Cooper, C. E., & Knowles, R. G. (2001). Nitric oxide synthases: Structure, function and inhibition. *Biochemical Journal*, *357*(3), 593-615.

Bharath, L. P., Ruan, T., Li, Y., Ravindran, A., Wan, X., Nhan, J. K., . . . Symons, J. D. (2015). Ceramide-initiated protein phosphatase 2A activation contributes to arterial dysfunction in vivo. *Diabetes*, *64*(11), 3914-3926.

Bonness, K., Aragon, I. V., Rutland, B., Ofori-Acquah, S., Dean, N. M., & Honkanen, R. E. (2006). Cantharidin-induced mitotic arrest is associated with the formation of aberrant mitotic spindles and lagging chromosomes resulting, in part, from the suppression of PP2A. *Molecular Cancer Therapeutics, 5*(11), 2727-2736.

Bornfeldt, K., & Tabas, I. (2011). Insulin resistance, hyperglycemia, and atherosclerosis. *Cell Metabolism*, *14*(5), 575-585.

Boyle, J. P., Thompson, T. J., Gregg, E. W., Barker, L. E., & Williamson, D. F. (2010). Projection of the year 2050 burden of diabetes in the US adult population: Dynamic modeling of incidence, mortality, and prediabetes prevalence. *Population Health Metrics*, *8*(1).

Chun, L., Junlin, Z., Aimin, W., Niansheng, L., Benmei, C., & Minxiang, L. (2011). Inhibition of ceramide synthesis reverses endothelial dysfunction and atherosclerosis in streptozotocin-induced diabetic rats. *Diabetes Research and Clinical Practice*, *93*(1), 77-85.

Foulkes, J. G. & Jefferson, L. S. (1984). Protein phosphatase-1 and -2A activities in heart, liver, and skeletal muscle extracts from control and diabetic rats. *Diabetes, 33,* 576-579.

Galbo, T., Perry, R. J., Nishimura, E., Samuel, V. T., Quistorff, B., & Shulman, G. I. (2013). PP2A inhibition results in hepatic insulin resistance despite Akt2 activation. *Aging, 5*(10), 770-781.

Geraldes, P., & King, G. L. (2010). Activation of protein kinase C isoforms and its impact on diabetic complications. *Circulation Research*, *106*(8), 1319-1331.

Götz, J., & Schild, A. (2003). Transgenic and knockout models of PP2A. *Methods in Enzymology Protein Phosphatases*, *366*, 390-403.

Holland, W. L., & Summers, S. A. (2008). Sphingolipids, insulin resistance, and metabolic disease: New insights from in vivo manipulation of sphingolipid metabolism. *Endocrine Reviews*, *29*(4), 381-402.

Kim, J. H., Kim, J., & Park, Y. (2012). Trans-10,cis-12 conjugated linoleic acid enhances endurance capacity by increasing fatty acid oxidation and reducing glycogen utilization in mice. *Lipids*, *47*(9), 855-863.

Lu, J., Kovach, J. S., Johnson, F., Chiang, J., Hodes, R., Lonser, R., & Zhuang, Z. (2009). Inhibition of serine/threonine phosphatase PP2A enhances cancer chemotherapy by blocking DNA damage induced defense mechanisms. *Proceedings of the National Academy of Sciences*, *106*(28), 11697-11702.

Lu, J., Zhuang, Z., Song, D. K., Mehta, G. U., Ikejiri, B., Mushlin, H., . . . Lonser, R. R. (2010). The effect of a PP2A inhibitor on the nuclear receptor corepressor pathway in glioma. *Journal of Neurosurgery*, *113*(2), 225-233.

Martiniova, L., Lu, J., Chiang, J., Bernardo, M., Lonser, R., Zhuang, Z., & Pacak, K. (2011). Pharmacologic modulation of serine/threonine phosphorylation highly sensitizes PHEO in a MPC cell and mouse model to conventional chemotherapy. *PLoS ONE*, *6*(2).

Matthews, D. R., Hosker, J. P., Rudenski, A. S., Naylor, B. A., Treacher, D. F., & Turner, R. C. (1985). Homeostasis model assessment: Insulin resistance and beta-cell function from fasting plasma glucose and insulin concentrations in man. *Diabetologia, 28*(7), 412-419.

Mehra, V. C., Jackson, E., Zhang, X. M., Jiang, X., Dobrucki, L. W., Yu, J., . . . Bender, J. R. (2014). Ceramide-activated phosphatase mediates fatty acid–induced endothelial VEGF resistance and impaired angiogenesis. *The American Journal of Pathology*, *184*(5), 1562-1576.

Mukhopadhyay, A., Saddoughi, S. A., Song, P., Sultan, I., Ponnusamy, S., Senkal, C. E., . . . Ogretmen, B. (2009). Direct interaction between the inhibitor 2 and ceramide via sphingolipid-protein binding is involved in the regulation of protein phosphatase 2A activity and signaling. *The FASEB Journal*, *23*(3), 751-763.

Sessa, W. C. (2004). ENOS at a glance. *Journal of Cell Science*, *117*(12), 2427-2429.

Shaul, P. W. (2002). Regulation of endothelial nitric oxide synthase: Location, location, location. *Annual Review of Physiology*, *64*(1), 749-774.

Shi, Y. (2009). Serine/threonine phosphatases: mechanism through structure. *Cell, 139,* 468-484.

Smith, A. R., Visioli, F., Frei, B., & Hagen, T. M. (2006). Age-related changes in endothelial nitric oxide synthase phosphorylation and nitric oxide dependent

vasodilation: Evidence for a novel mechanism involving sphingomyelinase and ceramide-activated phosphatase 2A. *Aging Cell*, *5*(5), 391-400.

Summers, S. A. (2010). Sphingolipids and insulin resistance: The five Ws. *Current Opinion in Lipidology*, *21*(2), 128-135.

Symons, J. D. (2013). Opportunity "Nox": A novel approach to preventing endothelial dysfunction in the context of insulin resistance. *Diabetes*, *62*(6), 1818-1820.

Symons, J. D., & Abel, E. D. (2013). Lipotoxicity contributes to endothelial dysfunction: A focus on the contribution from ceramide. *Reviews in Endocrine and Metabolic Disorders*, *14*(1), 59-68.

Symons, J. D., Mcmillin, S. L., Riehle, C., Tanner, J., Palionyte, M., Hillas, E., . . . Abel, E. D. (2009). Contribution of Insulin and Akt1 signaling to endothelial nitric oxide synthase in the regulation of endothelial function and blood pressure. *Circulation Research*, *104*(9), 1085-1094.

Triggle, C. R., & Ding, H. (2010). A review of endothelial dysfunction in diabetes: A focus on the contribution of a dysfunctional eNOS. *Journal of the American Society of Hypertension*, *4*(3), 102-115.

Wende, A. R., Symons, J. D., & Abel, E. D. (2012). Mechanisms of lipotoxicity in the cardiovascular system. *Current Hypertension Reports*, *14*(6), 517-531.

Wu, Y., Song, P., Xu, J., Zhang, M., & Zou, M. (2007). Activation of protein phosphatase 2A by palmitate inhibits AMP-activated protein kinase. *Journal of Biological Chemistry*, *282*(13), 9777-9788.

Zhang, Q., Holland, W. L., Wilson, L., Tanner, J. M., Kearns, D., Cahoon, J. M., . . . Symons, J. D. (2012). Ceramide mediates vascular dysfunction in diet-induced obesity by PP2A-mediated dephosphorylation of the eNOS-Akt complex. *Diabetes*, *61*(7), 1848-1859.

Zhang, Q., Mcmillin, S. L., Tanner, J. M., Palionyte, M., Abel, E. D., & Symons, J. D. (2009). Endothelial nitric oxide synthase phosphorylation in treadmill-running mice: Role of vascular signalling kinases. *The Journal of Physiology*, *587*(15), 3911-3920.

Zhu, Y., Pereira, R. O., O'neill, B. T., Riehle, C., Ilkun, O., Wende, A. R., . . . Abel, E. D. (2013). Cardiac PI3K-Akt impairs insulin-stimulated glucose uptake independent of mTORC1 and GLUT4 translocation. *Molecular Endocrinology*, *27*(1), 172-184.